Journal of Catalysis **195,** 227–236 (2000)
doi:10.1006/jcat.2000.3002, available online at http://www.idealibrary.com on IDEAL®

On the Mechanism of Alkane Isomerisation (Isodewaxing) with Unidirectional 10-Member Ring Zeolites. A Molecular Dynamics and Catalytic Study

German Sastre, Antonio Chica, and Avelino Corma[1]

Instituto de Tecnologia Quimica U.P.V.-C.S.I.C., Universidad Politecnica de Valencia, Avenida Los Naranjos s/n, 46022 Valencia, Spain

Received December 24, 1999; revised May 22, 2000; accepted July 18, 2000

Molecular dynamics techniques have been used to simulate the diffusion of *n*-heptane, 2-methyl-hexane, 2,3-dimethyl-pentane, 1-propyl-2-methyl-cyclopropane, and 1-isopropyl-2-methyl-cyclopropane in two unidimensional medium pore zeolites, ZSM-48 and Theta-1. In this way the isomerisation reactions *n*-heptane → 2-methyl-hexane → 2,3-dimethyl-pentane were studied, also including the cyclopropane reaction intermediates. The self-diffusivity of these sorbates and its variation with the channel size of the zeolite is studied. The diffusion in the slightly larger channels of ZSM-48 is faster than that found in Theta-1, and an effect of product shape selectivity, especially in Theta-1, is observed in the reaction going from the monomethyl to the dimethyl isomer. An excess of the monobranched/dibranched ratio is then expected in Theta-1 with respect to ZSM-48. The role of the external versus internal surface in the reaction products has been investigated by carrying out catalytic isomerisation of *n*-hexadecane in Theta-1 by depleting the external surface of acid sites. The results show that terminal monobranched alkanes can be formed inside the pores, and that dibranched alkanes are mainly formed at the external surface by isomerisation of the monobranched products.

Key Words: **molecular dynamics; zeolite; diffusion; shape selectivity; isodewaxing.**

1. INTRODUCTION

Reactions of alkanes in the area of petroleum refining, such as cracking, alkylation, dehydrogenation, isomerisation, and disproportionation, are catalysed by microporous solid acids (1–4). These reactions proceed via heterolytic bond cleavage, giving carbocations as intermediates or transition states (5–9). With monofunctional solid acid catalysts, carbocations are formed during the initiation step via protonation or hydryde abstraction of the alkane feed (10–13), and can then undergo isomerisation and β-scission. In the case of bifunctional catalysts a carbenium ion is formed by protonation of the olefin generated by dehydrogenation of the alkane on the metal component of the catalyst. The cracking/isomerisation ratio (C/I) depends on factors such as pore size, temperature, diffusivity, number, location, density, and strength of the acid centres (14–17).

The middle distillates in the synthesis of diesel are characterised by the cold flow properties such as pour point, viscosity, and freezing point (18), and to meet the required specifications the conversion of *n*-alkanes into their monobranched isomers is a desired process. Zeolites with 12 MR (member ring) channels can host mono-, di-, and tribranched hydrocarbons and the isomerisation process tends to give a considerable amount of the two latter (19, 20). More reasonable choices for isodewaxing are the zeolites with 10 MR pores where monobranched hydrocarbons diffuse, and dibranched alkanes may still diffuse but certainly with much greater restrictions than in 12 MR zeolites (21, 22). Diffusivity of the monobranched and dibranched products plays a crucial role as it determines the residence time inside the micropore structure which, when larger, favours the rate of cracking reactions with respect to isomerisation (19). Also, the C/I ratio increases with the temperature and chain length (23). Zeolites with 10 MR channels have been tested for hydroconversion processes and some mechanisms and general features have been found (16). With these zeolites branching of *n*-alkanes seems to occur to different extents in the terminal and internal positions of the molecule, and this effect is more pronounced as the diameter of the 10 MR channel decreases. In this regard, different yields of 3-methyl-hexane and 2-methyl-hexane have been observed in MTT zeotypes (24, 25).

The methyl shift isomerisation proceeds in 10 MR zeolites as a shape-selective process and the right choice of structure can direct the products towards the desired isomers. For instance, the channels of Theta-1 are sufficiently narrow so as to preclude the isomerisation of 3-methyl-hexane to 2-methyl-hexane (26). Shape selectivity is also responsible for a low isomerisation rate in TON and MTT zeotypes and this favours the occurrence of cracking, which is proved by the high yield of *n*-butane observed during C7 conversion (27). Theta-1 zeolite has been successfully tested

[1] To whom correspondence should be addressed. Fax: +34-96-387-7809. E-mail: acorma@itq.upv.es.

0021-9517/00 $35.00

for isodewaxing by monitoring the (terminal i-C7)/(internal i-C7) ratio which is obtained in excess of the thermodynamic ratio. The structure of Theta-1 gives a low amount of dibranched C7 whilst the monobranched isomers are easily formed (27).

Although a number of studies have made clear the general features of the 10 MR unidimensional zeolites in the hydroconversion of long- and medium-chain *n*-alkanes, discussions on the role of the external surface of the zeolite in the catalytic process are still open (28–32). Sometimes the catalytic results do not allow an unambiguous interpretation of whether the reaction occurs at the external surface (pore mouth catalysis) or inside the microporous structure (intracrystalline catalysis).

Three main explanations of the catalytic isomerisation in zeolite Theta-1 have been proposed: (a) Pore mouth catalysis (21, 24, 26, 30, 33), which predicts the formation of monobranched isomers with terminal methyl groups only at the external surface (pore mouth) of the microporous catalyst. According to this, the transition states of the isomerisation from linear to monobranched hydrocarbons are too bulky to be formed inside the channel structure, and then the formation of mono-, di-, and tribranched isomers can occur only at the external surface. (b) Transition state shape selectivity (24, 34, 35), which proposes that the transition state in the isomerisation from linear to monobranched alkanes with terminal methyl groups is about the size of the zeolite channels and therefore monobranched alkanes can be formed. Also, it is proposed that transition states leading to monobranched isomers without terminal methyl groups are bulkier and thus less favoured and they are produced to a significantly lesser extent. (c) Product shape selectivity (36–38), which suggests that monobranched isomers with terminal and internal methyl groups can both be formed inside the zeolite channel, although the latter diffuse more slowly and give more secondary reactions (i.e., cracking).

Computer simulation is a valuable tool which allows one to calculate the intracrystalline self-diffusion of the hydrocarbons involved, and from the results the different mechanisms of catalysis can be either confirmed or ruled out. Along this line, two recent studies by Webb *et al.* (39, 40) show the diffusivity of monomethyl-branched alkanes with respect to their corresponding linear isomers in zeotypes TON, EUO, MFI, FER, MEL, MTT, and AEL. As in previous studies, differences in diffusivity of the monomethyl-branched alkanes are observed in the narrower structures depending on the branching position. From those results it can be learned that small differences in the channel openings of 10 MR zeolites can render sensible changes in the product distributions.

In the present work we study the diffusion of linear, monobranched, and dibranched C7 alkanes in ZSM-48 and Theta-1 zeotypes by molecular dynamics simulations. We have also studied the diffusion of some cyclopropane (CP)

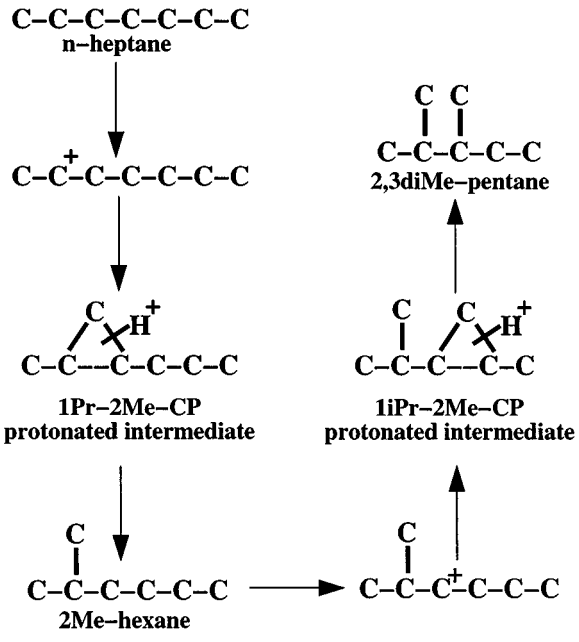

SCHEME 1. Isomerisation scheme of *n*-heptane to 2Me-hexane and 2,3diMe-pentane by the protonated cyclopropane mechanism.

derivatives of geometry similar to that of the protonated cyclopropanes obtained as intermediates in the isomerisation of *n*-heptane to 2-methyl-hexane (2Me-hexane), and 2-methyl-hexane to 2,3-dimethyl-pentane (2,3diMe-pentane). Scheme 1 shows the isomerisation reactions through the protonated cyclopropane intermediates. It is clear that not all of the possible isomers are studied here, and in particular the carbenium ion depicted after the formation of 2Me-hexane (Scheme 1) is not the most stable, but it is an intermediate for the formation of the 2,3diMe-pentane, which is the dimethyl isomer of interest in this study. The cyclopropanes considered are 1-propyl-2-methyl-cyclopropane (1Pr-2Me-CP) and 1-isopropyl-2-methyl-cyclopropane (1iPr-2Me-CP). The self-diffusion of these intermediate-like hydrocarbons is also studied in order to investigate whether possible restrictions to diffusion come from reactant, transition state, or product shape selectivity. From the catalytic viewpoint it is obvious that the formation of these transition states occurs in the active centre and therefore they do not diffuse through the microporous structure; nevertheless, the aim of studying the diffusion of these intermediates is to investigate the possible shape selectivity restrictions for them to be formed during the isomerisation reactions.

We have also carried out a catalytic study of the *n*-hexadecane isomerisation in Theta-1. Zeolite samples with different Al content at the external surface have been tested in order to assess the relative importance of the catalytic process at the external surface and inside the microporous structure.

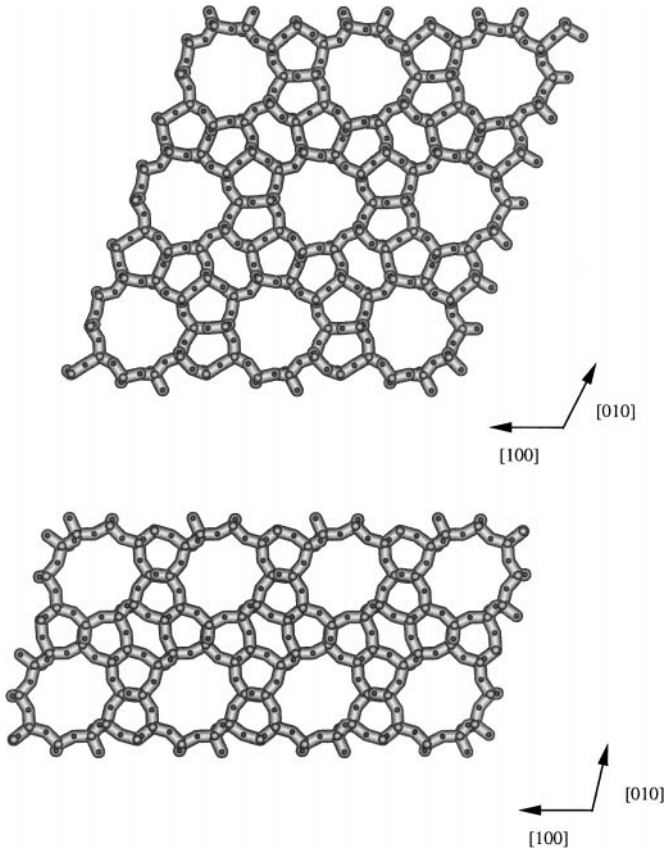

FIG. 1. View of the ZSM-48 (top) and Theta-1 (bottom) macrocells used in the simulations along the 10 MR channels.

2. METHODOLOGY

2.1. Molecular Dynamics Technique

Atomistic periodic molecular dynamics calculations have been carried out to simulate the diffusion of *n*-heptane, 2Me-hexane, 2,3diMe-pentane, 1Pr-2Me-CP, and 1iPr-2Me-CP in purely siliceous ZSM-48 (41) and Theta-1 (42) (TON-type (43)) zeolites (Fig. 1). The general purpose DL_POLY_2.11 (44) parallel code has been used all through this study.

The simulation proceeds by first assigning initial velocities to all atoms according to a Maxwell–Boltzmann distribution which depends on the temperature of the system. From this starting point, Newton's equations of motion are solved using a finite time step by means of the standard Verlet algorithm (45). A time step of 1 fs has been employed in the simulations.

The systems comprise (a) a $4 \times 2 \times 4$ macrocell of ZSM-48 (1944 atoms) plus nine molecules of hydrocarbons, and (b) a $4 \times 2 \times 4$ macrocell of Theta-1 (1152 atoms) plus eight molecules of hydrocarbons, to which parallelepiped periodic boundary conditions are applied. The geometry of the zeolite is first optimised at 0 K using the BFGS (46) technique implemented in the GULP (47) code and the result is used as input for a 25-ps equilibration stage of the zeolite + sorbate system at 450 K. The derivative of the energy with respect to the displacements is checked by the code to be below 100 kT/Å to avoid the collision between the atoms of the system during the equilibration period, and also the velocities are rescaled to keep the temperature constant. After the equilibration period, the velocity rescaling algorithm is removed and a run of 10 ps is performed to ensure that the temperature remains constant at 450 K within a fluctuation of ±5 K. After this period, runs of 300 ps were carried out within the NVE ensemble at 450 K.

During the simulation, configurations were saved every 250 steps, and subsequent analysis used the MSD facility included in DL_POLY to obtain mean square displacements (MSD) calculated according to the following expression (48).

$$\langle X^2(t)\rangle = \frac{1}{N_{\mathrm{m}} N_{t_0}} \sum_{t_0} \sum_{i} [X_i(t + t_0) - X_i(t_0)]^2, \qquad [1]$$

where N_{m} is the number of diffusing molecules, N_{t_0} is the number of time origins used in calculating the average, and X_i is the coordinate of the centre of mass of molecule i.

The diffusion coefficient, D, is then calculated using the Einstein relation (48):

$$\langle X^2(t)\rangle = 6Dt + B, \qquad [2]$$

where t is the simulation time, and B is the thermal factor arising from atomic vibrations.

As it is known that the MSD plots show an anomalous behaviour in the tail as a consequence of the poorer average at increasing simulation time (48), only the first 50 ps was taken into account to calculate the MSD. Nevertheless, it should be taken into account that the statistics of the full 300-ps simulation are necessary to characterise properly the slope of the first 50 ps. In other words, simulations of only 50 ps would not give sufficiently approximated diffusion coefficients.

The full motion of the framework atoms has been considered throughout the simulations. Although this increases substantially the computational expense, the influence of the framework flexibility has been made clear in a number of studies, especially when the sorbate matches the channel size (49–51), as is the case here. Also, the hydrocarbon atoms were allowed to move explicitly in order to optimise their conformation relative to the channel shape as the diffusion proceeds. A utility program was used to draw the hydrocarbon skeleton conformations at each step of the simulation and this served to visualise the conformations of the hydrocarbon as the diffusion takes place. The simulations were carried out on the 34 processors CRAY-T3E at CIEMAT, primarily using 16 processors.

TABLE 1

Atomic Charges (a.u.) of the Alkanes (See Figure 2) Used in the Coulombic Interactions (See Eqs. [6] and [7]) in the Molecular Dynamics Simulations

Atom	Hydrocarbon				
	n-Heptane	1Pr-2Me-CP	2Me-hexane	1iPr-2Me-CP	2,3diMe-pentane
C(primary)	−0.3306(2)	−0.3245(2)	−0.3238(3)	−0.3147(3)	−0.3256(4)
C(secondary)	−0.2076(5)	−0.2027(2)	−0.2047(3)	—	−0.2054(1)
C(sec-ring)[a]	—	−0.2678(1)	—	−0.2652(1)	—
C(tertiary)	—	—	−0.1233(1)	−0.1165(1)	−0.1141(2)
C(tert-ring)[b]	—	−0.1381(2)	—	−0.1349(2)	—
H	0.1062(16)	0.1088(10)	0.1068(16)	0.1088(10)	0.1085(16)
H(ring)[c]	—	0.1276(4)	—	0.1269(4)	—

Note. The number of atoms of each type is indicated between parentheses.

[a] This corresponds to a secondary carbon in the cyclopropane ring. See carbon 3 of 1Pr-2Me-CP, and carbon 4 of 1iPr-2Me-CP (Fig. 2).

[b] This corresponds to a tertiary carbon in the cyclopropane ring. See carbons 2 and 4 of 1Pr-2Me-CP, and carbons 3 and 5 of 1iPr-2Me-CP (Fig. 2).

[c] This corresponds to the hydrogens bonded to the carbons in the cyclopropane ring. See hydrogens bonded to carbon atoms 2, 3, and 4 of 1Pr-2Me-CP and carbon atoms 3, 4, and 5 of 1iPr-2Me-CP (Fig. 2).

2.2. Interatomic Potentials

Four types of interatomic potentials are used to model the systems:

$$V_{\text{total}} = V_{\text{zeolite}} + V_{\text{alkane}} + V_{\text{alkane–alkane}} + V_{\text{zeolite–alkane}}. \quad [3]$$

The parameter for the framework, V_{zeolite}, was taken from Catlow *et al.* (52), and is essentially a Born model potential comprising three terms:

$$V_{\text{zeolite}} = V_{\text{buck}} + V_{\text{three-body}} + V_{\text{coul}}. \quad [4]$$

The first term is a short-range splined Buckingham function for which a cut-off distance of 7.6 Å was used. A three-body, O–Si–O, nonharmonic potential in the form used by Catlow *et al.* (52) was chosen to describe bond angle-bending forces. Finally, the long-range electrostatic interactions were calculated by means of the Ewald summation technique, with a convergence criterion of 10^{-4} eV in the electrostatic energy, and using the charges +4.0 and −2.0 for silicon and oxygen, respectively.

The intramolecular potential for the sorbate, V_{alkane}, comprises four terms and was taken from Oie *et al.* (53):

$$V_{\text{alkane}} = V_{\text{two-body}} + V_{\text{three-body}} + V_{\text{four-body}} + V_{\text{coul}}. \quad [5]$$

The carbon atom parameters are different according to the location they have in the molecule, given as primary, secondary, or tertiary. The potential includes harmonic two-body and three-body bond-bending terms for the interactions C–C, C–H; and C–C–C, C–C–H, H–C–H, respectively. The four-body interaction is described by a cosine potential (53) for the quartets, C–C–C–C, C–C–C–H, and H–C–C–H.

Finally, 12-6 Lennard-Jones potentials and coulombic interactions were used to describe the intermolecular guest–guest and framework–guest interactions according to the following equations:

$$V_{\text{alkane–alkane}} = V_{\text{Lennard-Jones}} + V_{\text{coul}} \quad [6]$$

$$V_{\text{zeolite–alkane}} = V_{\text{Lennard-Jones}} + V_{\text{coul}}. \quad [7]$$

The guest–guest terms included were C–C, C–H, and H–H. As for framework–guest interactions, the terms included were C–O and H–O. The parameters were taken from Catlow *et al.* (52). Partial charges for the carbon and hydrogen atoms are listed in Table 1.

2.3. Experimental

Starting from a commercial sample of Theta-1 supplied by BP Amoco, three different samples have been obtained by dealumination with HCl. The dealumination has been carried out in a stirred autoclave with a 5 M aqueous solution of HCl and a ratio of 10 ml of HCl per gram of zeolite, at a temperature of 140°C during a period of 1–5 h. The crystallinity of the samples was preserved upon the acid treatments. The acidity of the resultant samples was characterised by pyridine and di-*tert*-butylpyridine adsorption and the results are given in Table 2. The reaction was carried out in a continuous fixed-bed reactor at a pressure of 10^6 Pa, 3.34 WHSV, and a molar ratio of H_2/HC of 155. The results obtained are shown in Table 3 for conversion levels of 30% and 50%.

3. RESULTS AND DISCUSSION

3.1. Optimisation of the Zeolite Frameworks

The all-silica (SiO_2 composition) zeolite frameworks ZSM-48 (41) and Theta-1 (42) (Fig. 1) were optimised and

TABLE 2

Acidity Measured by Pyridine and Di-*tert*-butyl-pyridine (DTBP) Desorption in the Samples of Theta-1

	Desorption temp (°C)	T1	T1A	T5A
Brønsted[a]	250	40	38	35
	350	36	30	22
Lewis[a]	250	3	3	4
	350	3	3	4
DTBP[b]	150	2.80	1.40	1
Si/Al (chemical analysis)		38	48	55

[a] Micromoles of pyridine adsorbed per gram of catalyst.
[b] Relative intensity of the $DTBPy^+$ band.

TABLE 4

Cell Parameters of the Experimental and Optimised ZSM-48 and Theta-1 Zeolites

	ZSM-48		Theta-1	
Cell parameter	Exp.[41]	Optim.[a]	Exp.[42]	Optim.[b]
a (Å)	14.240	14.443	13.859	13.871
b (Å)	20.140	20.358	17.420	17.410
c (Å)	8.400	8.516	5.038	5.003
α (°)	90.0	90.0	90.0	90.0
β (°)	90.0	90.0	90.0	90.0
γ (°)	90.0	90.0	90.0	90.0

[a] The optimisation was performed within the *Cmcm* space group.
[b] The optimisation was performed within the $Cmc2_1$ space group.

the resulting crystallographic parameters are close to those found by X-ray diffraction (Table 4). The ZSM-48 structure chosen for our simulations corresponds to the UUDD stacking (also UDUD would be possible) and this structure resembles that of the straight channels of ZSM-5 (43). These structures present a unidimensional system of nonintersecting channels with 10 MR openings and the corresponding window openings are 5.6×5.3 Å and 5.5×4.4 Å in ZSM-48 and Theta-1, respectively. The relative channel dimensions are therefore ZSM-48 > Theta-1. Although this will be used to justify the self-diffusivities obtained, it has to be borne in mind that the fluctuations in window sizes can make these dimensions change by ~0.5 Å due to the thermal vibrations and the flexibility of the lattice (54), and this will be taken into account by performing flexible framework molecular dynamics. Once the structures have been optimised the hydrocarbons are introduced into the 10 MR channels with the following loadings: 9 hydrocarbons in the $4 \times 2 \times 4$ macrocell of ZSM-48, and 8 hydrocarbons in the $4 \times 2 \times 4$ macrocell of Theta-1. The number of 10 MR channels in the zeolite macrocells is 12 in ZSM-48 and 10 in Theta-1, and the hydrocarbons have been introduced by avoiding having more than one in each channel of the macrocell. This means that each hydrocarbon would interact only through alkane–alkane interactions with its translational image along the channel in the contiguous macrocells. Then, taking into account that the channel lengths in the macrocells are 24.94 Å and 20.01 Å in ZSM-48 and Theta-1, respectively, it follows that the current loadings are equivalent to infinite dilution as the intermolecular interactions have been cut off at 7.6 Å. Increasing loadings could change the self-diffusivity of the hydrocarbons, but in this study only the effect of the interaction between the structure and the hydrocarbon is taken into account in order to figure out the shape selectivity of these zeolites towards the different degree of hydrocarbon branching. The hydrocarbons can change the C–C–C–C dihedrals as they diffuse and this flexibility influences the self-diffusion coefficients. The hydrocarbons are shown in Fig. 2.

TABLE 3

Catalytic Behaviour for the Hydroisomerisation of *n*-hexadecane with Theta-1 Samples under Different Reaction Conditions

	T1		T1A		T5A	
Sample, temp. (°C)	267	275	268	276	270	276
% Conversion	30.0	50.0	30.0	50.0	30.0	50.0
% Isomerisation	27.8	43.4	27.4	42.4	26.8	42.8
% Selectivity	92.5	86.8	91.5	84.8	89.3	85.5
% 2-MB	33.8	30.7	37.2	30.2	37.8	35.8
% 3-MB	15.9	15.7	14.6	15.7	15.5	15.9
% 4-MB	8.7	8.8	7.5	8.8	7.7	8.1
% 5-MB	10.4	10.6	10.3	10.7	10.0	10.3
% 6-MB	9.6	10.0	10.4	10.6	9.6	9.8
% 7-MB + 8-MB	17.5	18.3	17.2	18.0	16.6	17.1
% (2+3)/(4+5+6+7+8)	1.07	0.97	1.14	0.95	1.21	1.14
% DB	4.1	5.8	2.9	6.1	2.7	3.2

Note. MB, monobranched; DB, dibranched.

3.2. Self-diffusion Coefficients of Linear, Monobranched, Dibranched, and Intermediate-like C7 Alkanes in ZSM-48 and Theta-1

The diffusion coefficients are obtained from the molecular dynamics simulations (see Eqs. [1] and [2]) and they give a quantitative description of the self-diffusivity. Mean square displacements of 2Me-hexane, 1Pr-2Me-CP, *n*-heptane, 1iPr-2Me-CP, and 2,3diMe-pentane are given for ZSM-48 and Theta-1 (Fig. 3), and the corresponding diffusion coefficients are shown in Table 5.

3.2.1. Small-size alkanes: n-heptane and 1Pr-2Me-CP. It can be seen that there are two hydrocarbons diffusing noticeably faster than the others: *n*-heptane and 1Pr-2Me-CP, the main structural difference between them being the presence of a cyclopropane ring in the latter (Fig. 2). The small size of the cyclopropane ring does not pose a

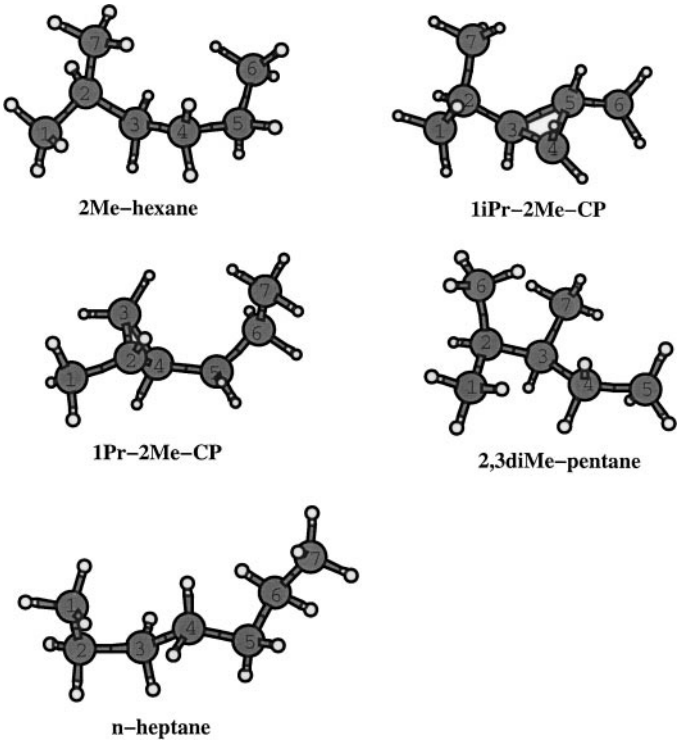

FIG. 2. Hydrocarbons used in the simulations: 2Me-hexane, 1Pr-2Me-CP, *n*-heptane, 1iPr-2Me-CP, and 2,3diMe-pentane. The rotation around the C–C–C–C dihedrals allows different conformations as the hydrocarbons diffuse. The figures correspond to a random conformation adopted during the simulation and they show geometries that differ from the minimum energy conformation. In particular it is shown from the figures of *n*-heptane and 1Pr-2Me-CP that the C–C–C–C rotation in the former makes it of similar size compared to the latter and this is of interest to explain their relative self-diffusivities. Analogously, the sizes of 1iPr-2Me-CP and 2,3diMe-CP are similar.

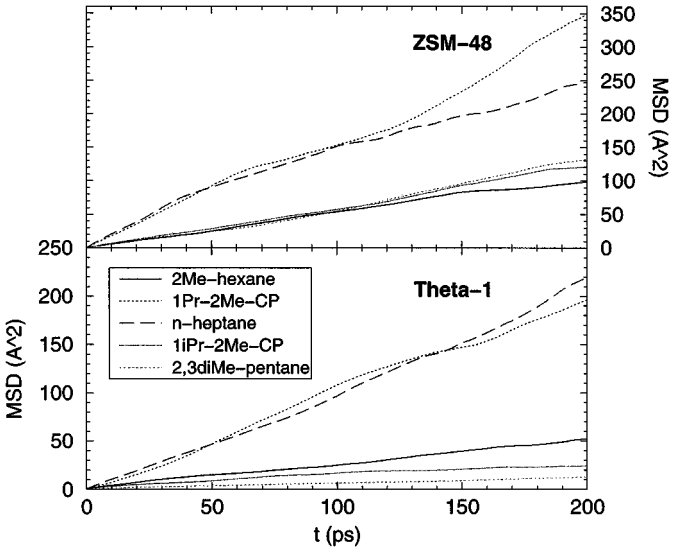

FIG. 3. Mean square displacement plots of 2Me-hexane, 1Pr-2Me-CP, *n*-heptane, 1iPr-2Me-CP, and 2,3diMe-pentane in ZSM-48 (top) and Theta-1 (bottom). Although the simulations have been extended to 300 ps, only the first 200 ps is shown in the graph. The self-diffusion coefficients calculated from these plots (see Eq. [2]) are shown in Table 5.

limitation to the diffusion of the 1Pr-2Me-CP with respect to *n*-heptane, as can be seen from the respective coefficients, 30.8×10^{-6} and 31.2×10^{-6} cm^2/s, and 15.2×10^{-6} and 15.3×10^{-6} cm^2/s in ZSM-48 and Theta-1, respectively (Table 5). The large diffusivity of 1Pr-2Me-CP is due to the rigidity of the cyclopropane ring which precludes excessive *folding* of the hydrocarbon as it diffuses. Despite the small size of these two alkanes which causes them to fit loosely in the zeolite channels, a decrease in the diffusivity by a factor of 2 is observed when going from ZSM-48 to Theta-1 (Table 5) due to the narrower channels of the latter. This trend is expected to be more pronounced as the sorbate size increases.

3.2.2. Medium-size alkanes: 2Me-hexane and 1iPr-2Me-CP. The diffusivity of these hydrocarbons is smaller than that of the previous alkanes (*n*-heptane and 1Pr-2Me-CP), and larger than that of the dibranched isomer, 2,3diMe-CP (Table 5). The difference in self-diffusivity with respect to the small-size alkanes suggests that the isomerisation from linear to monobranched isomers may be partially controlled by the diffusivity of the products. In this regard, small differences in the channel sizes may lead to important differences in the self-diffusivity of the monobranched products due to the fact that some diffusional restraints appear, and in fact a reduction factor of 1.6 (from 7.8×10^{-6} to 4.8×10^{-6} cm^2/s) is found in the respective coefficients of 2Me-hexane in ZSM-48 and Theta-1 (Table 5). Another interesting aspect is that in ZSM-48 the diffusivity of the 1iPr-2Me-CP is larger than that of 2Me-hexane and this may be due to the fact that the cyclopropane ring makes the 1iPr-2Me-CP molecule more rigid, avoiding excessive *folding* as it diffuses through the void space of ZSM-48, thus making its diffusivity slightly larger than that of 2Me-hexane. On the other hand, in Theta-1 the opposite behaviour is observed, and the diffusivity of 2Me-hexane is larger than that of the 1iPr-2Me-CP (Table 5) and this may be due to the fact that the narrower channels of Theta-1

TABLE 5

Self-Diffusion Coefficients (cm^2/s) of the Alkanes in ZSM-48 and Theta-1 at 450 K Obtained from the MSD Plots in Fig. 3

Sorbate	ZSM-48	Theta-1
n-Heptane	31.213×10^{-6}	15.316×10^{-6}
1Pr-2Me-CP	30.795×10^{-6}	15.193×10^{-6}
2Me-hexane	7.820×10^{-6}	4.823×10^{-6}
1iPr-2Me-CP	9.221×10^{-6}	2.431×10^{-6}
2,3diMe-pentane	7.709×10^{-6}	1.027×10^{-6}

are imposing more restraint on the methyl branch plus the cyclopropane ring present in 1iPr-2Me-CP with respect to the 2Me-hexane which has only the methyl branch and can better *optimise* its conformation as it diffuses. This indicates that a transition state shape selectivity effect appears in the 2Me-hexane → 2,3diMe-pentane reaction in Theta-1, whereas this will not be the case in ZSM-48 (where the transition state, 1iPr-2Me-CP, still has a diffusion coefficient of 9.2×10^{-6} cm^2/s, as can be seen from Table 5).

The effect of a decreasing channel size from ZSM-48 to Theta-1 is more noticeable in the diffusivity of the bulkier 1iPr-2Me-CP (with respect to 2Me-hexane) whose coefficient decreases by a factor of 3.8 (from 9.2×10^{-6} to 2.4×10^{-6} cm^2/s, see Table 5), whereas in the case of 2Me-hexane the decreasing factor is only 1.6 (from 7.8×10^{-6} to 4.8×10^{-6} cm^2/s, see Table 5).

3.2.3. Dibranched alkane: 2,3diMe-pentane. For the bulkier 2,3diMe-pentane a self-diffusivity very similar to that of the monobranched 2Me-hexane is observed in ZSM-48 (Table 5). This feature is somewhat surprising but it is explained by taking into account that the channels of ZSM-48 are still of sufficient size so as to allow the optimisation of the conformation of both isomers. The dibranched 2,3diMe-pentane can then *optimise* its conformation, making the two methyl groups not to point in opposite directions, and this makes its size only slightly larger than that of the monobranched 2Me-hexane. The situation is different in Theta-1, and the larger size of the dibranched isomer determines its diffusivity with respect to the monobranched 2Me-hexane. As stated above, a diffusion restraint was already observed in Theta-1 when going from *n*-heptane to 2Me-hexane (the self-diffusivity decreases by a factor of 3.2); this effect is more marked when going from 2Me-hexane to 2,3diMe-pentane (the self-diffusivity decreases by a factor of 4.7). Therefore, it appears that the narrower channels of Theta-1 are more selective for the isomerisation reactions considered, and this will cause the isomerisation reactions to be more controlled by diffusion in Theta-1 than in ZSM-48.

Our study does not cover all the possibilities of dibranched isomers to be formed and in this regard dibranched alkanes with nonneighbour ramifications are expected to diffuse better than when the two ramifications are neighbours (35). Therefore, we are not excluding here the possibility of formation of dibranched isomers in Theta-1 as long as the methyl branches are far apart in the molecule. Nevertheless, from our diffusivity results for 2,3diMe-pentane it follows that little yield of this isomer will be expected in Theta-1 compared to the yield of monobranched products.

3.2.4. Discussion on diffusion coefficients. Other molecular dynamics simulations show a more marked effect regarding the drop in diffusivity when passing from linear to monobranched alkanes. Webb *et al.* (40), using static lattice molecular dynamics, obtain diffusion coefficients of 146.8×10^{-6} and 17.2×10^{-6} cm^2/s for *n*-heptane and 2Me-hexane in Theta-1 at 600 K respectively; this meaning a decrease by a factor of 8.5, which is larger than the factor of 3.2 obtained from Table 5. Experimental measurements by PFG-NMR have been conducted only on linear alkanes and they show diffusion coefficients of 7.0-, 3.9-, and 1.2×10^{-6} cm^2/s for *n*-butane, *n*-pentane, and *n*-hexane in silicalite at 333 K, with a loading of 4 molecules per unit cell (55). A recent computational study (56) using a rigid zeolite also showed more than 1 order of magnitude of difference in the diffusion coefficients of *n*-butane and *i*-butane in ZSM-22 at 333 K (18.80×10^{-6} and 0.01×10^{-6} cm^2/s, respectively). Our simulations have been done considering a flexible zeolite framework; i.e., all the atoms of the frame have been optimized. This, in principle, should be a better approximation than considering a fixed framework. Nevertheless, it appears that even if the trend for the diffusion coefficients obtained with the level of hydrocarbon branching is correct, the absolute differences are probably too small. In any case we have considered here those values only on a relative basis of obtain tendencies.

3.3. Catalytic Results with Theta-1

3.3.1. Formation of monobranched isomers. The results for the *n*-hexadecane isomerisation in Theta-1 shown in Table 3 point to a similar activity for the three samples dealuminated at different levels, corresponding to reaction temperatures of 267–270°C (to obtain 30% conversion), and of 275–276°C (to obtain 50% conversion). The similarity in the activities of the three samples is surprising if one takes into account that the Si/Al ratio was increased from 38 to 55 by the acid treatments. However, the activity results seem more logical if one takes into account that the acidity measured by pyridine, especially after desorbing at 250°C, is also very similar on the three samples. The explanation of why the acidity measured by pyridine adsorption decreases much less than one would expect from the values of the zeolite Si/Al ratios can be extracted by looking by IR at the evolution of the bridging hydroxyl groups of the three samples before and after adsorbing pyridine, as well as at the difference spectra of the before and after spectra, which gives the amount of bridging hydroxyls interacting with pyridine (Fig. 4). The spectra show that not all bridging groups were reached by the pyridine and what is important for our discussion is that the proportion of the accessible sites increases when carrying out the acid treatment to increase the Si/Al ratio. It appears that on the one hand the dealumination process decreases the number of potential acid sites, but on the other hand it increases the proportion of the accessible ones probably due to a better diffusion of the pyridine when the number of sites is smaller, and/or to the removal of extraframework species that may partially block some of the channels. In any case, we see that the small decrease in activity parallels the small decrease

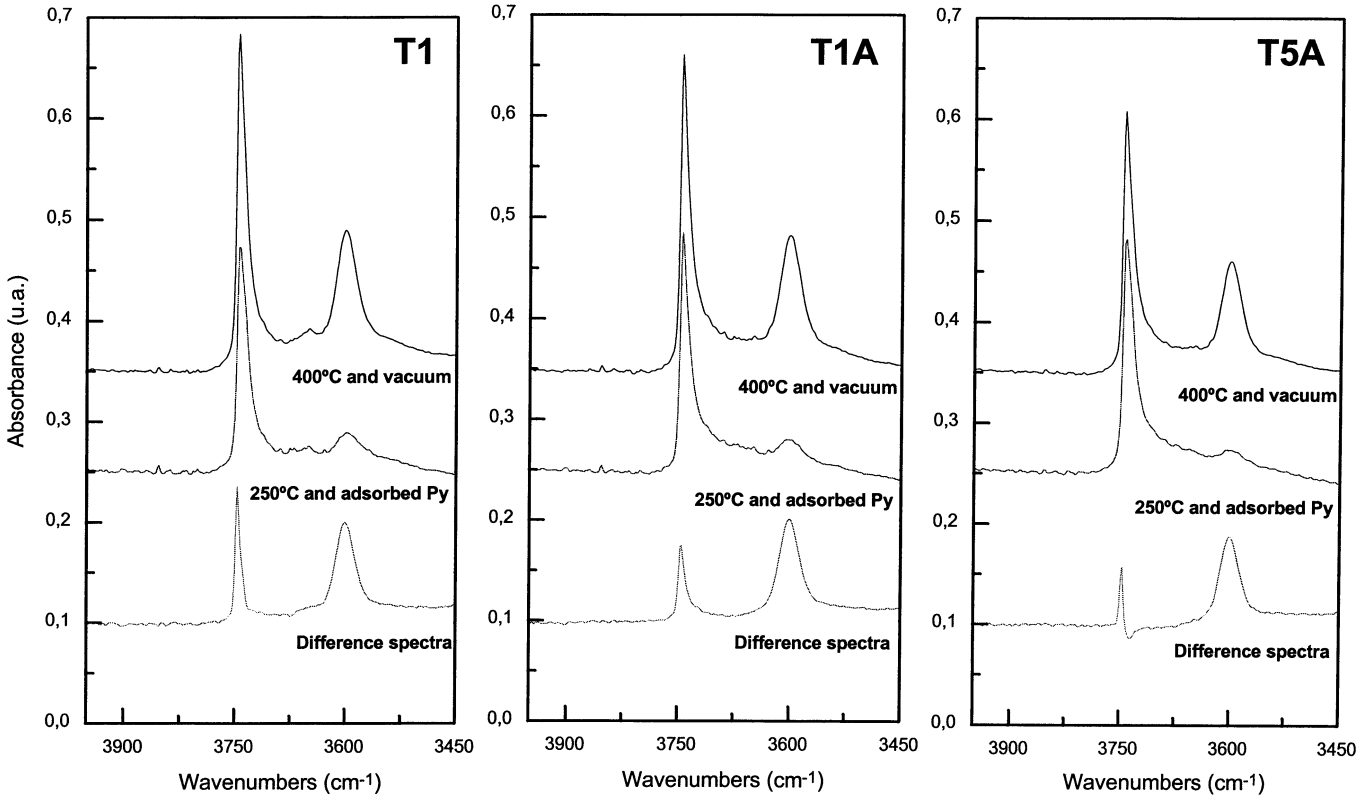

FIG. 4. Evolution of the bridging hydroxyl groups, measured by IR, before and after adsorbing pyridine together with the difference IR spectra for the three dealuminated samples of Theta-1 zeolite.

in acidity measured by pyridine, especially at 250°C, and furthermore the pyridine sees a larger proportion of the total bridging hydroxyl groups. This is an indication that *n*-hexadecane should also interact with most of the acid sites and consequently isomerization can also occur inside the channels.

If one considers now the adsorption of di-*tert*-butylpyridine, that should interact with acid sites only at the external surface and close to the pore mouth, we can see that the amount of di-*tert*-butylpyridine (DTBPy) adsorbed, unlike that of pyridine, is strongly reduced upon dealumination. The DTBPy results indicate that, as expected, the dealumination process occurred to a large extent at the external surface or, in other words, a framework Al gradient concentration in the zeolite crystallites has been established where the Si/Al ratio should decrease from the outer to the inner part of the zeolite crystal.

It is obvious that if the formation of the monobranched products would take place mainly on acid sites close to the external surface, a very strong decrease in activity should occur upon the dealumination performed here. However, the decrease in catalytic activity and more specifically in isomerisation (Table 3) is rather small and is in better agreement with the global acidity measured by pyridine adsorption. From these results we have to conclude that an important part of the monobranching isomerisation should occur deep inside the pore channels of the Theta-1 zeolite (Scheme 2).

It has been reported that the 3- and especially the 2-methyl isomers are clearly favoured with this zeolite (26). Then, if we accept that monomethyl isomers are formed mainly inside the pores and moreover that the *n*-alkane–*n*-alkene should diffuse in single file with the molecule elongated, it appears that the isomerisation at the second and third carbons should be more favourable to occur from a geometrical point of view, taking into account the geometries of the transition state and the zeolite pore. Moreover, the higher product selectivity of 2Me-pentadecane with respect to the other monobranched isomers can also be due to the larger intracrystalline diffusivity of the former, as has been calculated by Webb *et al.* (39, 40).

If one looks closely at the monobranched isomer distribution (Table 3) it appears that the ratio of (2-+3-MB)/(4-+5-+6-+7-+8-MB) methyl-pentadecane isomers increases when depleting the Al from the external part of the crystallites. This would support the conclusion that the monobranched isomers other than 2- and 3-pentadecane are formed to a relatively larger extent than the two terminal branched isomers on the external surface of the Theta-1 zeolite (Scheme 2).

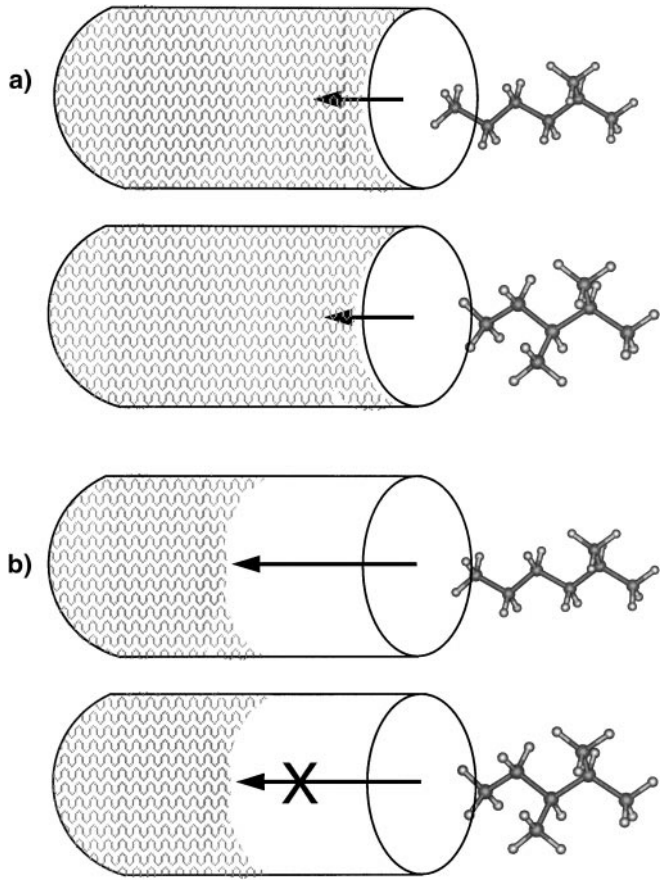

SCHEME 2. Isomerisation in the external surface of the micropore. (a) Monobranched and dibranched alkanes can isomerise in the external surface if the acid centres are located near the external surface. (b) If the acid centres are located more internally in the catalyst, the terminal monobranched can reach the centres more easily than the other bulkier isomers, and therefore the dibranched isomers will be formed at the expense of the terminal monobranched. The acid centre location is indicated by the pattern.

3.3.2. Formation of dibranched isomers. In the case of dibranched products it can be seen (Table 3) that the yield decreases with decreasing external acidity. This is an indication that dibranched alkanes are formed mainly at the external surface of the Theta-1 zeolite. This is in agreement with our simulations that show significantly lower diffusion coefficients for dibranched than for monobranched alkanes in Theta-1 (Table 5), as well as with the existence of serious geometrical restrictions for the formation of dibranched products (especially those with vecinal methyl groups) within the pores of the zeolite.

4. CONCLUSIONS

Molecular dynamics techniques have been used to simulate the diffusion of 2Me-hexane, 1Pr-2Me-CP, *n*-heptane, 1iPr-2Me-CP, and 2,3diMe-pentane in two medium-pore zeolites, ZSM-48 and Theta-1. These hydrocarbons are the C7 alkanes involved in the isomerisation reactions: *n*-heptane → 2Me-hexane → 2,3diMe-pentane. Also, two cyclopropane alkanes whose geometries resemble that of the protonated cyclopropane isomerisation intermediates were simulated.

The secondary reaction from monobranched to dibranched alkanes (from 2Me-hexane to 2,3diMe-pentane in this case) is the most interesting in ZSM-48 and Theta-1. In ZSM-48 the reactant, transition state, and product diffuse to a considerable extent. In Theta-1 the reaction is more controlled by diffusion due to both transition state and product constraints imposed by the narrower channels of Theta-1 with respect to those of ZSM-48. A higher yield of monomethyl with respect to dimethyl isomers is expected in Theta-1.

Both channel systems of ZSM-48 and Theta-1 seem more appropriate for isodewaxing than, for example, the narrower 10 MR channels of MCM-22 where a previous computer simulation study gives a self-diffusion coefficient of 6.81×10^{-6} cm^2/s for *n*-heptane at 550 K (57), and a much smaller diffusivity for the 2Me-hexane, thus precluding isomerisation to branched products. In this study, a diffusion coefficient of 4.82×10^{-6} cm^2/s is observed for 2Me-hexane in Theta-1, which indicates that terminal monobranched isomers diffuse without serious restraints in Theta-1, and also its formation should not be restricted by transition state shape selectivity as long as the 1Pr-2Me-CP intermediate shows a large diffusivity. On the other hand, it is the dibranched isomer, 2,3diMe-pentane, which shows diffusion restraints in Theta-1, and this points to a marked effect of product shape selectivity.

The catalytic results in the Theta-1 samples in which the external acid centres have been depleted show that terminal monobranched isomers are formed mainly deep inside the microporous space, and that dibranched alkanes are formed mainly at the external surface. The terminal monobranched alkanes can also diffuse out to the external surface once formed in the intracrystalline micropore, and isomerise to dibranched alkanes when an acid centre is located near the external surface.

ACKNOWLEDGMENTS

We thank CICYT of Spain for the project MAT-97-1016-C02-01. The CIEMAT (Centro de Investigaciones Energeticas, Medio Ambientales y Tecnologicas) is acknowledged for the use of the CRAY-T3E. G.S. thanks Dr. W. Smith for useful discussions regarding the DL_POLY code. The suggestions made by the referees are gratefully acknowledged.

REFERENCES

1. Corma, A., *Chem. Rev.* **95**, 559 (1995).
2. Corma, A., and Martinez, A., *Adv. Mater.* **7**, 137 (1995).
3. Rabo, J. A., *Catal. Today* **22**, 201 (1994).
4. Weitkamp, J., *Catal. Today* **19**, 107 (1994).

5. Corma, A., Planelles, J., Sanchez-Marin, J., and Tomas, F., *J. Catal.* **93**, 30 (1985).
6. Jentoft, F. C., and Gates, B. C., *Topics Catal.* **4**, 1 (1997).
7. Kazansky, V. B., *Acc. Chem. Res.* **24**, 379 (1991).
8. van Santen, R. A., and Kramer, G. J., *Chem. Rev.* **3**, 637 (1995).
9. Boronat, M., Viruela, P., and Corma, A., *J. Phys. Chem. B* **101**, 10069 (1997).
10. Sie, S. T., *Ind. Eng. Chem. Res.* **31**, 1881 (1992).
11. Sie, S. T., *Ind. Eng. Chem. Res.* **32**, 397 (1993).
12. Sie, S. T., *Ind. Eng. Chem. Res.* **32**, 403 (1993).
13. Wojciechowski, B. W., and Corma, A., "Catalytic Cracking: Catalysts, Chemistry and Kinetics." Dekker, New York, 1986.
14. Corma, A., *in* "Zeolite Microporous Solids: Synthesis, Structure, and Reactivity" (E. G. Derouane, *et al.*, Eds.), p. 373. Kluwer, Dordrecht, 1992.
15. Weitkamp, J., "Hydrocracking and Hydrotreating," ACS Symp. Series 20, p. 1. Am. Chem. Soc., Washington, DC, 1975.
16. Martens, J. A., and Jacobs, P. A., *Zeolites* **6**, 334 (1986).
17. Guisnet, M., and Lukyanov, D., *Stud. Surf. Sci. Catal.* **90**, 367 (1990).
18. Bennet, R. N., and Elkes, G. J., *Oil Gas J.* **3**, 69 (1975).
19. Corma, A., Fornes, V., Monton, J. B., and Orchilles, A. V., *J. Catal.* **107**, 288 (1987).
20. Smirniotis, P. J., and Ruckenstein, E., *Ind. Eng. Chem. Res.* **33**, 800 (1994).
21. Miller, S. J., *Microporous Mater.* **2**, 439 (1994).
22. Nace, D. M., *Ind. Eng. Chem. Prod. Res. Dev.* **8**, 31 (1969).
23. Martens, J. A., Parton, R., Uytterhoeven, L., Jacobs, P. A., and Froment, G. J., *Appl. Catal.* **76**, 95 (1991).
24. Maesen, Th. L., Schenk, M., Vlugt, T. J. H., de Jong, J. P., and Smit, B., *J. Catal.* **188**, 403 (1999).
25. Meriaudeau, P., Tuan, V. A., Hung, L. N., Nghiem, V. T., and Naccache, C., *J. Chem. Soc., Faraday Trans.* **94**, 467 (1998).
26. Ernst, S., Weitkamp, J., Martens, J. A., and Jacobs, P. A., *Appl. Catal.* **48**, 137 (1989).
27. Gianetto, G. E., Perot, G. R., and Guisnet, M. R., *Ind. Eng. Chem. Prod. Res. Dev.* **25**, 481 (1986).
28. Martens, J. A., Souverijns, W., Verrelst, W., Parton, R., Froment, G. J., and Jacobs, P. A., *Angew. Chem., Int. Ed. Engl.* **34**, 2528 (1995).
29. Meriaudeau, P., Tuan, V. A., Lefebvre, F., Nghiem, V. T., and Naccache, C., *Microporous Mesoporous Mater.* **26**, 161 (1998).
30. Souverijns, W., Martens, J. A., Uytterhoeven, L., Froment, G. J., and Jacobs, P. A., *Stud. Surf. Sci. Catal.* **105**, 1285 (1997).
31. Denayer, J. F., Baron, G. V., Vanbutsele, G., Jacobs, P. A., and Martens, J. A., *Chem. Eng. Sci.* **54**, 3553 (1999).
32. Souverijns, W., Martens, J. A., Froment, G. J., and Jacobs, P. A., *J. Catal.* **174**, 177 (1998).
33. Claude, M. C., and Martens, J. P., *J. Catal.* **190**, 39 (2000).
34. Meriaudeau, P., Tuan, V. A., Saplay, G., Nghiem, V. T., and Naccache, C., *in* "Proceedings of the 12th International Zeolite Conference" (M. M. J. Treacy, B. K. Marcus, M. E. Bisher, and J. B. Higgins, Eds.), Vol. 4, p. 2913. Materials Research Society, Warrendale, PA, 1999.
35. Meriaudeau, P., Tuan, V. A., Nghiem, V. T., Sapaly, G., and Naccache, C., *J. Catal.* **185**, 435 (1999).
36. Frasch, M. V., Kazansky, V. B., Rigby, A. M., and van Santen, R. A., *J. Phys. Chem. B* **101**, 5346 (1997).
37. Natal-Santiago, M. A., Alcala, R., and Dumesic, J. A., *J. Catal.* **181**, 124 (1999).
38. Radom, L., Hariharan, P. C., Pople, J. A., and Schleyer, R. J., *J. Am. Chem. Soc.* **95**, 6531 (1973).
39. Webb, E. B., and Grest, G. S., *Catal. Lett.* **56**, 95 (1998).
40. Webb, E. B., Grest, G. S., and Mondello, M., *J. Phys. Chem. B* **103**, 4949 (1999).
41. Marler, B., *Zeolites* **7**, 393 (1987).
42. Schlenker, J. L., Rohrbaugh, W. J., Chu, P., Valyocsik, E. W., and Kokotailo, G. T., *Zeolites* **5**, 355 (1985).
43. Meier, W. M., Olson, D. H., and Baerlocher, Ch., "Atlas of Zeolite Structure Types" 4th Ed. Elsevier, Amsterdam, 1996. Also on the Web: http://www.iza-sc.ethz.ch/IZA-SC/Atlas/AtlasHome.html.
44. Smith, W., and Forester, T. R., *J. Mol. Graphics* **14**, 136 (1996).
45. Verlet, L., *Phys. Rev.* **159**, 98 (1967).
46. (a) Broyden, C. J., *J. Inst. Math. Appl.* **6** 222 (1970); (b) Fletcher, R., *Comput. J.* **13**, 317 (1970); (c) Goldfard, D., *Math. Comput.* **24**, 23 (1970); (d) Shanno, D. F., *Math. Comput.* **24**, 647 (1970).
47. Gale, J. D., *J. Chem. Soc., Faraday Trans.* **93**, 629 (1997).
48. Allen, M. P., and Tildesley, D., "Molecular Simulation of Liquids." Oxford Univ. Press, London, 1980.
49. Demontis, P., Suffritti, G. B., Quartieri, S., Fois, E. S., and Gamba, A., *Zeolites* **7**, 522 (1987).
50. Dumont, D., and Bougeard, D., *Zeolites* **15**, 650 (1995).
51. Sastre, G., Catlow, C. R. A., and Corma, A., *J. Phys. Chem. B* **103**, 5187 (1999).
52. Catlow, C. R. A., Freeman, C. M., Vessal, B., Tomlinson, S. M., and Leslie, M. J., *J. Chem. Soc., Faraday Trans.* **87**, 1947 (1991).
53. Oie, T., Maggiora, T. M., Christoffersen, R. E., and Duchamp, D. J., *Int. J. Quantum Chem., Quantum Biol. Symp.* **8**, 1 (1981).
54. Sastre, G., Cano, M. L., Corma, A., Garcia, H., Nicolopoulos, S., Gonzalez-Calbet, J. M., and Vallet-Regi, M., *J. Phys. Chem. B* **101**, 10184 (1997).
55. Heink, W., Kärger, J., Pfeifer, H., Datema, K. P., and Nowak, A. K., *J. Chem. Soc., Faraday Trans.* **88**, 3505 (1992).
56. Schuring, D., Jansen, A. P. J., and van Santen, R. A., *J. Phys. Chem. B* **104**, 941 (2000).
57. Sastre, G., Catlow, C. R. A., Chica, A., and Corma, A., *J. Phys. Chem. B* **104**, 416 (2000).